DETECTION AND APPLICATION OF SULFUR HEXAFLUORIDE IN POWER EQUIPMENT BASED ON MID INFRARED TDLAS

Zekun CUI[1], Mingzhao HAN[2], Bing GAO[3], Lijuan GAO[4]

To enhance sulfur hexafluoride gas detection sensitivity and identify small leaks in power equipment, this study analyzes SO_2F_2, SOF_2, and SO_2 infrared spectra using Fourier transform infrared spectroscopy. A 2nd harmonic signal extraction method is proposed, incorporating a virtual lock-in amplifier. A tunable semiconductor laser gas detection simulation evaluates modulation effects, while an improved noise reduction algorithm enhances signal clarity. Experimental results show a strong linear correlation ($R^2 > 0.98$) between 2nd harmonic amplitude and gas concentration. The system demonstrated stability under constant temperature, with detection limits of 0.008 μL/L (SO_2F_2), 0.0055 μL/L (SOF_2), and 0.0019 μL/L (SO_2). This method significantly improves signal denoising, sensitivity, and stability, aiding in sulfur hexafluoride leak prevention and reducing maintenance costs. It has broad applications in power equipment gas safety detection.

Keywords: TDLAS; Sulfur hexafluoride; Infrared spectrometer; Power equipment; Testing

1 Introduction

Electrical equipment is an important component of the power system, and its reliability is crucial for the safety and stability of the power grid. Gas Insulated Switchgear (GIS) is widely utilized in power systems because of its high safety and compact structure [1-2]. Sulfur hexafluoride (SF_6) is an inorganic compound that appears as a stable non combustible gas at room temperature and pressure. Its electrical insulation strength is 2.5 times that of air under atmospheric pressure, and its arc extinguishing ability is over 100 times that of air [3]. Since the 1960s, SF_6 has been widely adopted in the power industry, particularly in transmission and

* Corresponding author
1 Development Planning Department, State Grid Hengshui Electric Power Supply Company, Hengshui 053000, China, email: cuizekkkun@outlook.com
2 Substation Maintenance Center, State Grid Hengshui Electric Power Supply Company, Hengshui 053000, China
3 Comprehensive Service Branch, State Grid Hengshui Electric Power Supply Company, Hengshui 053000, China
4 Development Planning Department, State Grid Hengshui Electric Power Supply Company, Hengshui 053000, China

distribution equipment such as GIS, because of its excellent insulation and arc extinguishing performance. It has now become the most commonly used insulation gas in ultra-high voltage and extra high voltage power systems [4]. In recent years, the number of composite electrical appliances of State Grid Corporation of China has steadily increased, and the total installed capacity has exceeded 2000 GW. The goal of building a smart grid is gradually being achieved. By detecting the decomposition components of SF_6, insulation defects in GIS equipment can be diagnosed, the operating status of the equipment can be understood, and the probability of equipment failure can be reduced [5]. The use of SF_6 decomposition components for diagnosing internal faults in power equipment has become a current research hotspot. Chu J et al. obtained SF_6 decomposition products of different types and contents by simulating spark and corona discharge. It established a fault recognition model using a recognition algorithm based on Stacked Denoising Autoencoder (SDAE) and used a gas sensitive nano material microsensor array to identify fault characteristic gases. This model demonstrated high detection accuracy [6]. Wang et al. proposed an improved fiber-reinforced Raman spectroscopy that combines a spatially filtered iris diaphragm and a reflector to enhance Raman signals, with detection limits as low as 1×10^{-6}~8×10^{-6}. Using SF_6 as the internal standard gas, multi-gas quantification of samples in 800 kV GIS was achieved with a maximum error of 5.5%. This technology was expected to provide a new approach for trace gas analysis in the power industry [7]. Cheng H et al. studied the typical insulation defect SF_6 decomposition behavior of the valve side bushing of gas-solid insulated converter transformers under partial discharge and compared it with gas insulated switchgear. The decomposition of SF_6 varied depending on the type of insulation defect. The ratio of CO_2 and SO_2 under metal protrusion defects was affected by whether the needle tip was wrapped in epoxy resin impregnated paper [8]. Kaiyuan LI et al. proposed an open optical path fire detection system based on Tunable Diode Laser Absorption Spectroscopy (TDLAS) and laser remote sensing to extract CO signals through wavelength modulation spectroscopy and replace the traditional absorption measurement chamber with a laser with a wavelength of 2331.93 nm. The experimental results show that the system is stable at different reflectance, distance and Angle, and the detection limit is 20~88.22 (μL/L)·m [9].

Tunable Diode Laser Absorption Spectroscopy (TDLAS) can selectively detect the characteristic absorption lines of gas molecules, providing high sensitivity and accuracy for gas concentration measurement. This has wide applications in environmental monitoring, industrial process control, and medical diagnosis. Relevant scientific research and technical personnel have conducted extensive work on the research and application of TDLAS detection technology in different fields. Zhang Q et al. proposed a high-sensitivity and high reliability diode laser absorption spectroscopy gas detection system based on temperature pressure compensation algorithm for detecting CH_4 concentration in near space. This

algorithm improved the detection accuracy of the sensor, with a linear correlation coefficient r^2 of 0.9990 [10]. Chang J et al. used wavelength modulation spectrum and tunable diode laser absorption spectrum to construct an oxygen monitoring system based on LabVIEW, using 760.8nm laser and 3.3m Herriott battery. The experiment shows that the minimum detection limit of the system is 0.247% (the average time is 1 s), and the detection limit is reduced to 0.022% when it is extended to 40 s, so as to achieve high sensitivity oxygen detection [11]. De S et al. analyzed the R1f/ΔI1 wavelength modulated spectroscopy (WMS) technique, which enables multi-gas detection without calibration under complex conditions. Through the normalization of linear intensity modulation, this method can reduce the influence of light intensity change on the signal. Using 40mW, 1531.52nm semiconductor laser to extract acetylene, single-channel structure detection sensitivity of 0.32ppm, integration time of 58 seconds, significantly better than R2fWMS 1.53ppm limit, 4.7 times higher [12]. Xu Y et al. developed a self-calibrating fiber optic photoacoustic gas analyzer based on 2f/1f WMS, utilizing multi-pass absorption enhancement technology. The laser oblique design and high reflectors improve the absorption of gases and solids. The 1f and 2f signals are demodulated by a two-channel phase-locked white interferometer. The methane detection showed that the minimum detection limit was 20 ppb when integrating for 60 seconds. Even if the laser power is halved, the detection error is still within 3%, which is suitable for high-precision trace gas detection [13]. Kong W et al. designed a fiber enhanced Raman spectroscopy (FERS) technology based on silicon noise suppression, which uses anti-resonant fiber and hybrid filtering technology to reduce 90% noise and increase sensitivity by 4.22 times. The system achieved the detection limits of CF_4 to 1.34 ppmv and CO_2 to 1.44 ppmv, respectively. It identified the characteristic peak locations of C5F10O and its decomposed gas, and successfully dynamically monitored trends in the decomposed gas content of C5F100 GIPE, demonstrating the efficiency and stability of FERS in gas detection [14].

In summary, significant progress has been made in SF_6 gas detection research in power equipment, but there are still shortcomings. The SDAE fault recognition model and gas sensitive nano material microsensor array have improved detection accuracy but are susceptible to interference in complex environments. Fiber reinforced Raman spectroscopy has a low detection limit, but high equipment and operational requirements increase cost and complexity. The online monitoring of photoacoustic spectroscopy technology has the advantages of high accuracy and short time, but it needs to be optimized to adapt to different equipment. QEPAS and WMS methods may not be able to accurately distinguish the interference between sulfur hexafluoride and other gases in the face of complex gas mixtures. In addition, the normalization of WMS and the matrix change filtering of QEPAS may not completely eliminate the interference of multi-component background. These factors make it need to be further optimized to meet the high

precision requirements when it is applied in power equipment. TDLAS technology exhibits excellent performance in SF_6 detection in the Mid Infrared (MI) spectral region, shows potential in low concentration gas detection, and can maintain high stability under temperature and pressure changes. Based on the above analysis, this study uses the TDLAS system to analyze and detect the infrared spectra of gases such as SOF, SOF_2, SO_2, etc., and determines their detectable bands. It innovatively establishes a virtual Lock-in Amplifier (LiA) circuit and a TDLAS absorption simulation model and deeply explores the TDLAS gas detection process. Subsequently, a SF decomposition component detection platform based on MI TDLAS is built, and SO_2F_2, SOF_2, and SO_2 detection experiments are conducted. This study aims to improve the reliability of detecting small leaks in power equipment, avoid equipment damage due to leaks, and thus extend its service life.

2. Methods and Materials

This study uses the Fourier Transform Infrared Spectroscopy Detection Platform (FTISDP) to obtain infrared spectral data of SO_2F_2, SOF_2, and SO_2, and compares it with the spectral information of SO_2F_2 and SO_2 in the NIST database. The extraction method of second harmonic is studied, and the principles of different LiAs are analyzed. The virtual LiA structure for extracting Second Harmonic Signals (SHS) is determined. By building a TDLAS gas detection simulation platform for simulation, the influence of different modulation coefficients and modulation frequencies on SHS extraction is analyzed. An improved Complete Ensemble Empirical Mode Decomposition with Adaptive Noise (CEEMDAN) algorithm is adopted to denoise the noise signals in the TDLAS system.

2.1. Virtual LiA design based on LabVIEW

In the TDLAS gas detection system, spectral data containing gas concentration information is obtained by scanning the absorption band of the gas, and determining the output band of the light source is crucial. Infrared spectroscopy includes near-infrared, MI, and far-infrared. The molecular basic vibration transition frequency in the MI band is several orders of magnitude higher than the harmonic or combined frequency in the near-infrared band, making the MI band sensitivity more suitable for qualitative and quantitative analysis [15]. This study utilizes FTISDP to obtain and analyze the infrared spectra of SO_2F_2, SOF_2, and SO_2, and validates them with data from the NIST database [16]. The detection platform includes Thermo Scientific Nicolet iS50 infrared spectrometer, computer, long path gas cell, digital pressure gauge, detection bag, and vacuum pump. The system framework is shown in Fig. 1.

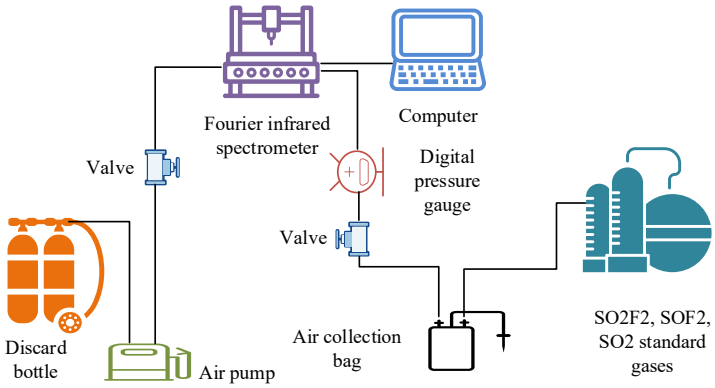

Fig. 1 Framework of Fourier infrared spectroscopy detection system

In Fig. 1, SO_2F_2, SOF_2, and SO_2 standard gases were used for gas infrared spectroscopy measurements in the experiment. Firstly, perform a gas washing operation on the gas pool with background gas, evacuate until the pressure gauge displays a vacuum state, fill in background gas, and repeat twice to eliminate impurities. Subsequently, background gas was introduced to collect spectral data. After the background gas collection is completed, extract the background gas, connect it to the gas to be tested, and perform vacuum treatment. After completing the gas washing, introduce the gas to be tested again to collect spectral data. After each spectral acquisition, repeat the gas washing operation and collect spectral data of different gases in sequence. SHS is positively correlated with gas concentration, and detecting SHS can effectively reflect gas concentration. Usually, LiA is used to process and extract SHS, which is separated from the original detection signal through phase sensitive detection. Orthogonal LiA adds a reference signal channel for orthogonal processing, eliminating the impact of phase difference on the system [17-18]. The orthogonal LiA structure is shown in Fig. 2.

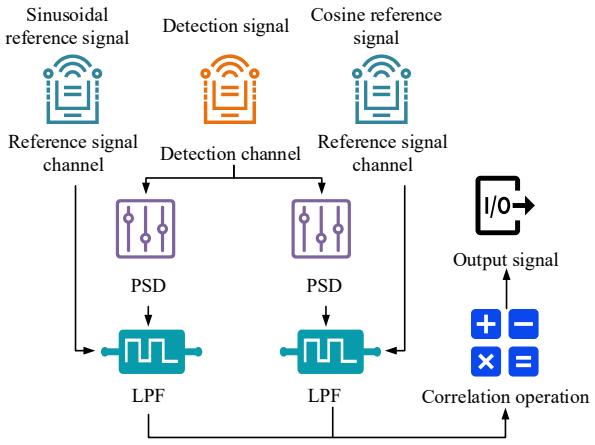

Fig. 2 Basic structure of orthogonal phase-locked amplifier

In Fig. 2, Low-pass Filter represents (LPF), Phase Sensitive Detector means PSD. orthogonal LiA has two reference signal channels and one detection signal channel. The phase difference between the reference signals of the two reference signal channels is 90 degrees. After entering the amplifier, the reference signal and detection signal undergo phase sensitive detection and filtering processing, which is consistent with the single channel LiA. After filtering, the signal is subjected to vector operation to gain the last signal. The calculation process of the final output is equation (1).

$$y(t)=\sqrt{y_s^2+y_c^2}=\frac{1}{2}AB \tag{1}$$

In equation (1), A and B are reference signals, and y_s is the signal to be measured. By processing the detection signal y_c with orthogonal LiA, errors caused by phase differences between the detection signal and the reference signal can be reduced, debugging workload can be reduced, and system detection sensitivity can be improved. In the TDLAS system, the detection sensitivity, accuracy, and lower limit are not only affected by system performance, but also by the environment and equipment. Environmental noise and instrument noise can interfere with detection signals, affecting signal processing and detection accuracy. When a detector detects light signals, it generates quantum fluctuations, known as shot noise. The shot noise increases with the increase of light intensity, but the Signal-to-Noise Ratio (SNR) improves. The calculation process of granular noise i_x is represented by equation (2).

$$i_x=\sqrt{\frac{2e^2\eta WP}{h\nu}} \tag{2}$$

In equation (2), high-frequency modulation signals can effectively suppress $1/f$ noise and reduce its impact on the detection results. The root mean square current of $1/f$ noise is equation (3).

$$i_{1/f}=\frac{e\eta P}{h\nu}\sqrt{\frac{B}{f}} \tag{3}$$

Thermal noise is generated by the random motion of charge carriers or electrons caused by the Brownian motion of charged particles in a conductive medium, which can form shot noise. Particle noise can be divided into two categories: one is caused by the emission of charge carriers or electrons inside active devices, and the other is caused by resistance thermal noise due to random fluctuations in current or voltage in circuits. The thermal noise current is equation (4).

$$i_r=\sqrt{\frac{4kTW_1}{R}} \tag{4}$$

In equation (3), R is the equivalent resistance. W_1 is the bandwidth of

thermal noise. k is the Boltzmann constant. T is temperature. The total noise of the photodetector is equation (5).

$$i^2 = i_s^2 + i_{1/f}^2 + i_r^2 \tag{5}$$

Noise is directly proportional to the detection bandwidth, and the impact of noise can be reduced by reducing the detection bandwidth or using noise reduction algorithms. Increasing the detection frequency can effectively suppress $1/f$ -noise. The instability of laser power is called laser additional noise. In the TDLAS system, optical interference fringe noise is caused by mirror reflection and beam interference, which affects detection performance. Although optimizing the optical path design can reduce the influence of stripes, it cannot completely eliminate them. In semiconductor lasers, the intensity (i.e. amplitude) of the output light not only depends on the input current, but is also affected by internal and external noise sources. Residual amplitude modulation noise manifests as random fluctuations in the intensity of laser output light, which can interfere with the stability and accuracy of the signal. It can be eliminated by background subtraction method [19]. The methods to reduce noise include selecting high-quality lasers and high-sensitivity detectors, and performing signal filtering. Most instruments in the LabVIEW program control library are designed based on the performance of real instruments, which can quickly build instrument platforms and conduct related research [20]. This study utilizes virtual LiA based on LabVIEW and uses orthogonal vector LiA as the theoretical basis to achieve the extraction and processing of SHS. The structure of virtual LiA is shown in Fig. 3.

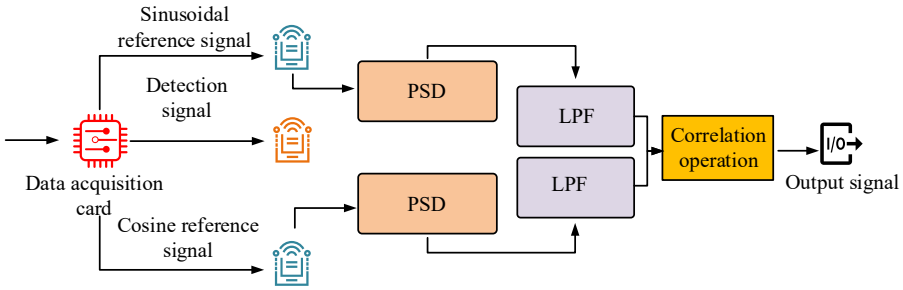

Fig. 3 Structure of virtual phase-locked amplifier

In Fig. 3, the detection signal is converted into an electrical signal by a photodetector and transmitted to the virtual LiA through a Data Acquisition Card (DAC). Its input includes detection, reference sine, and reference cosine signal ports. The reference signal is offered by the DAC to ensure consistency with the output modulation signal. After performing phase sensitive detection on the detection signal and reference signal in virtual LiA, the signal is transmitted to an infinite impulse response IIR Butterworth LPF for filtering, extracting the amplitude and phase of the relevant signal, and finally outputting SHS.

2.2. Design of SF_6 decomposition component detection model based on MI TDLAS

Based on the LabVIEW software mentioned above, a simulation model of TDLAS gas detection is constructed to simulate the process of TDLAS. The model consists of four parts, including the Quantum Cascade Laser (QCL) laser output module, absorption line function module, gas chamber module, and 2nd harmonic detection module. Through these modules, a comprehensive simulation of the TDLAS detection has been completed. The overall structure of the model is shown in Fig. 4.

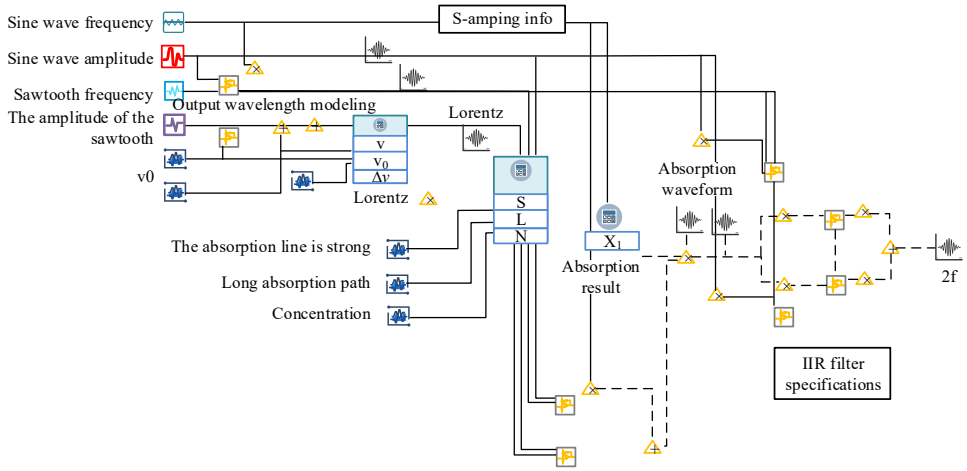

Fig. 4 TDLAS simulation model

When using TDLAS for gas concentration detection, in addition to the impact of detection system performance, it is also affected by environmental noise and instrument noise interference. Therefore, after extracting SHS, it is necessary to analyze and process the noise in the signal. Empirical Mode Decomposition (EMD) is an adaptive processing method suitable for nonlinear and non-stationary signals. Its main advantage is strong adaptability, which can effectively remove noise. However, EMD suffers from pattern aliasing and limitations, which may lead to errors and loss of time scales during the denoising process. Therefore, it is necessary to improve the EMD algorithm to enhance its noise reduction performance. To solve the mode mixing problem caused by noise and algorithm limitations in EMD decomposition, CEEMDAN introduces adaptive noise and reduces the impact of noise and Intrinsic Mode Function (IMF) component alignment problem through multiple stacking and optimized set averaging method, achieving high-precision signal reconstruction. ICEEMDAN enhances signal decomposition and reconstruction performance through further optimization, obtaining more accurate and stable modal components with minimal residual noise. The specific steps: the detection signal is assumed as a, and E_k is the k-th order

IMF component. m is the local mean, and $w^{(i)}(i=1,2,\ldots,N)$ is the added white noise. φ_0 is the standard deviation of white noise. i sets of white noise are added to the original sequence, and sequence $a^{(i)}$ is constructed to obtain the first set of residuals R_1. The specific formula for calculating the first modal component is equation (6).

$$d_1 = a - R_1 \tag{6}$$

The addition of white noise is continued, and the residual $a_1 + \varphi E\left(w^{(i)}\right)$ of the second group is solved. The second modal component is set to d_2. The above process is repeated, and the modal component d_k is obtained by calculating the k-th residual R_k, as shown in equation (7).

$$\begin{cases} R_k = \left(m\left(R_{k-1} + \varphi_{k-1} E\left(w^{(i)}\right)\right)\right) \\ d_k = R_{k-1} - R_k \end{cases} \tag{7}$$

By using the ICEEMDAN algorithm for decomposition, the residual noise in the IMF components can be significantly improved, and the problem of mean error caused by different numbers of IMF components generated by EEMD decomposition can be solved. Compared with EMD, EEMD, CEEMD, and CEEMDAN, ICEEMDAN has significant advantages. Therefore, this article adopts this method to denoise the second harmonic data containing noise. After determining the signal reconstruction range, useful IMF components are selected based on the principle of energy priority. The SF_6 decomposition component detection platform built on MI TDLAS is shown in Fig. 5, including laser, gas chamber, laser driver, photodetector, DAC, and computer.

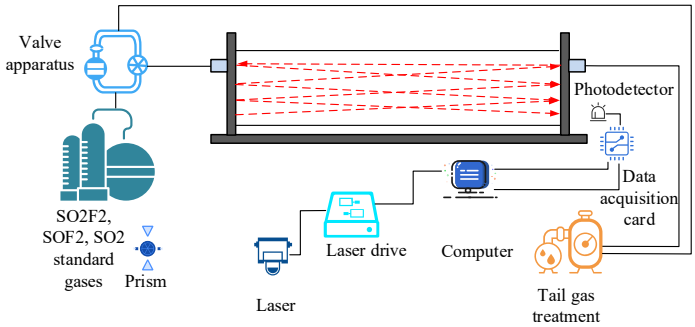

Fig. 5 TDLAS experimental system

In Fig. 5, in the SF6 decomposition product detection device of TDLAS system, Prism is mainly used to adjust and guide the laser path. By changing the propagation direction of the laser, it can better enter the gas chamber, thus ensuring that the gas to be measured can effectively absorb the laser. The precise control of the prism enables the modulated laser beam to interact with the target gas molecules

efficiently, improving the detection sensitivity and the overall stability of the system. This study generates and outputs a modulated signal that combines sine waves and sawtooth waves using the LabVIEW program. This signal is transmitted to the laser driver through the DAC. The laser driver sets the temperature and current of the laser to determine the output band of the laser. The laser is controlled to emit laser with modulation signal into the gas pool. The gas to be tested absorbs laser energy in a specific wavelength band, forming an absorption depression on the modulation signal. The photodetector detects the laser absorbed by the gas, converts it into an electrical signal, and transmits it to the DAC, which then uploads the signal to the computer. The LabVIEW virtual LiA module in the computer extracts the 2nd harmonic in the detection signal and uses the ICEEMDAN algorithm to denoise it. In this TDLAS system, the gas cell serves as the detection environment for the gas to be tested, using a Herriott optical gas cell with multiple reflections. The photodetector converts the detected optical signal into an electrical signal and transmits it to the DAC. This article uses the P13894 high-speed response and high sensitivity infrared detector produced by Hamamatsu Photonics Co., Ltd. In the system, the generation of high-frequency modulation signals and the acquisition of detection signals are completed by the Zishu USB4012 high-speed DAC to ensure effective signal generation and acquisition.

3. Results

The P13894 infrared detector used in the experiment has a detection cutoff wavelength of 11 μm, a noise equivalent power of 1.5×10^{-9}W/Hz$^{1/2}$, a sensitivity of 0.0019A/W, and a detection rate of 6.5×10^{7}cm·Hz$^{1/2}$/W. The detector is used in conjunction with the MI laser drive equipment from Novo Optics. This driving device integrates temperature control and current control functions. The experiment also used Zishu USB4012. In the experiment, the GC400 dynamic gas analyzer was used to prepare different concentrations of SO_2F_2, SOF_2 and SO_2 standard gases. Under normal circumstances, the uncertainty of a standard gas is about ±2%. The dynamic gas analyzer provides highly accurate gas control and mixing capabilities, generally within the ±1% range, to ensure the reliability of the standard gas concentrations produced. Table 1 shows the main configurations of the relevant equipment.

Table 1

Parameters of laser drive device and DAC

Laser drive parameter		DAC parameters	
Driving current/Maximum Driving Current (A)	±15/1	Maximum sampling rate (MS/s)	1.6
Temperature control range (℃)	-30~50	Single-ended output channel	8
Modulation bandwidth (kHz)	0~500	Input range (V)	±5 /±10
Temperature control accuracy (A)	≤ 0.01	Absolute accuracy (FSR)	0.005%

Drive current (V)	5~48	Digital to analog module resolution (bit)	12
Constant current voltage range (μA)	≤ 10	Adc module resolution (bit)	16

To compare the noise reduction effect of the ICEEMDAN, this section uses the noisy SHS obtained in the previous section, and performs noise reduction processing using EMD, CEEMD, and CEEMDAN algorithms, respectively. The noise reduction effects of each algorithm are compared and analyzed. Meanwhile, the SHS SNR of different filtering methods is compared, as shown in Fig. 6.

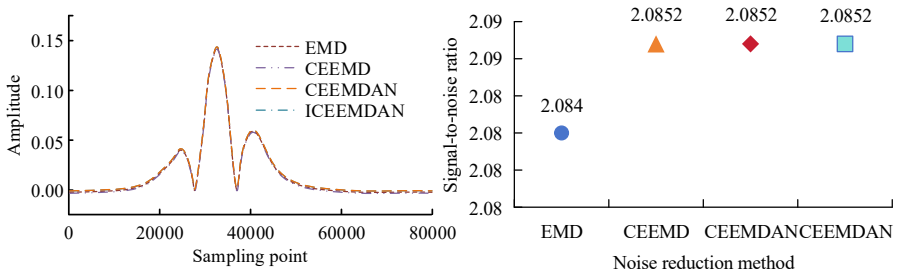

(a) Filtered spectrum of SHS (b) SHS`s SNR

Fig. 6 Performance comparison results of different filtering methods

The SHS spectrum in Fig. 6 represents the SF6 (sulfur hexafluoride) decomposition products, including SOF2 and SO2 spectral data. In Fig. 6 (a), after using these denoising methods, the noise of the original SHS is reduced to varying degrees. After various algorithmic processing, SHS has shown significant improvement compared to noisy signals, with an increase in the smoothness of the SHS. However, there are still some fluctuations in the amplitude of the SHS. In 6 (b), the SNR of SHS after ICEEMDAN denoising is 2.0856, which is higher than other EMD denoising algorithms. Using ICEEMDAN to remove noise in SHS can help improve the sensitivity of the detection system and reduce its detection limit, thereby better meeting the accurate detection requirements for trace amounts of SO_2F_2, SOF_2, and SO_2. Overall, ICEEMDAN performs well in SHS denoising, improving the SNR of the signal and effectively enhancing the performance. To study the platform's detection performance for SO_2F_2, SOF_2, and SO_2, 50 uL/L of SO_2F_2, SOF_2, and SO_2 standard gases are used in the experiment. Different concentrations of SO_2F_2, SOF_2, and SO_2 gases are prepared using a GC400 dynamic gas analyzer for detection. According to the simulation results, a 50kHz sine wave with a modulation factor of 2.1 is used to modulate the signal. The experiment is conducted at a constant temperature of 25 ℃. Before testing, 500 mL/min high-purity nitrogen is used to clean the gas and absorb it for several minutes to remove impurities. After cleaning, SO_2F_2, SOF_2, and SO_2 gases of different concentrations are introduced into the gas absorption cell at a flow rate of 500 mL/min. After a few minutes to ensure that the gas filled the cell, detection begins. Optical signals are

collected using photoelectric sensors and displayed on the upper computer. The original signal waveforms of the three gases are shown in Fig. 7.

In Fig. 7 (a), as the concentration of SO_2F_2 increases, the waveform amplitude decreases, and the waveform gradually decreases within the range of 2000-3500, which can be used for SO_2F_2 concentration detection. Fig. 7 (b) shows that the waveform of the SOF_2 raw signal deepens with increasing concentration and absorption depression, with a clear trend in the range of 2000-3200, which can be used for SOF_2 detection. Fig. 7 (c) shows that the absorption depression of SO_2 in the range of 3250-4000 deepens with increasing concentration, and SHS can be extracted for SO_2 detection. To detect the concentration of each gas within a certain range, its SHS is extracted. 1000 Second Harmonic Amplitude (SHA) data points are collected for each concentration of each gas, and the mean is taken as the detection value for concentrating to reduce the effect of isolated samples. Fig. 8 shows the fitting curves of the SHA detection values for SO_2F_2, SOF_2, and SO_2 gases with different concentrations.

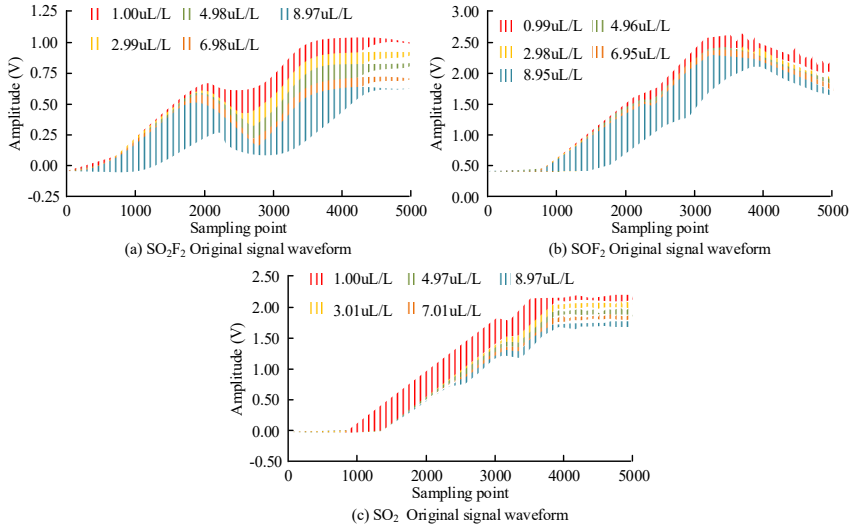

Fig. 7 Original signal waveforms of the three gases

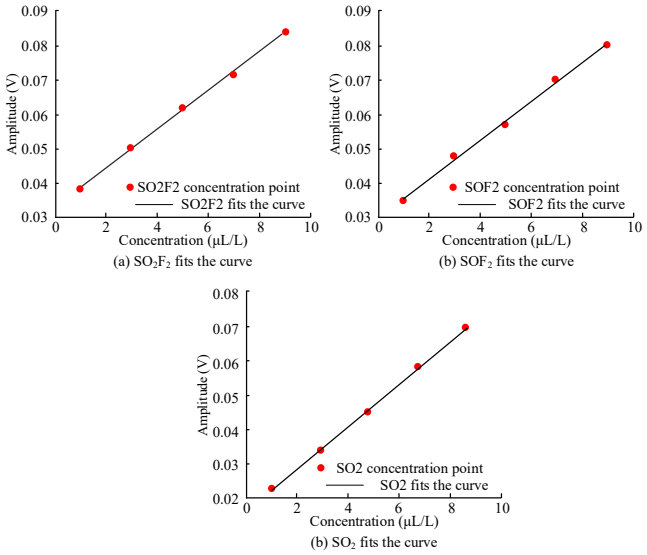

Fig. 8 Fitting curves of SO2F2, SOF2 and SO2 gases with different concentrations

In Figs. 8 (a) to (c), the goodness of fit between the SHA detection values of SO_2F_2, SOF_2, and SO_2 gases and their concentrations reached 0.999, 0.998, and 0.999, respectively. This indicates that the obtained SHA detection value has an excellent linear relation with gas concentration. In summary, there is a highly linear relationship between SHA and gas concentration, and the goodness of fit is above 0.98, which verifies the reliability and accuracy of the detection method. Fig. 9 shows the detection error analysis of the fitting curves for each gas.

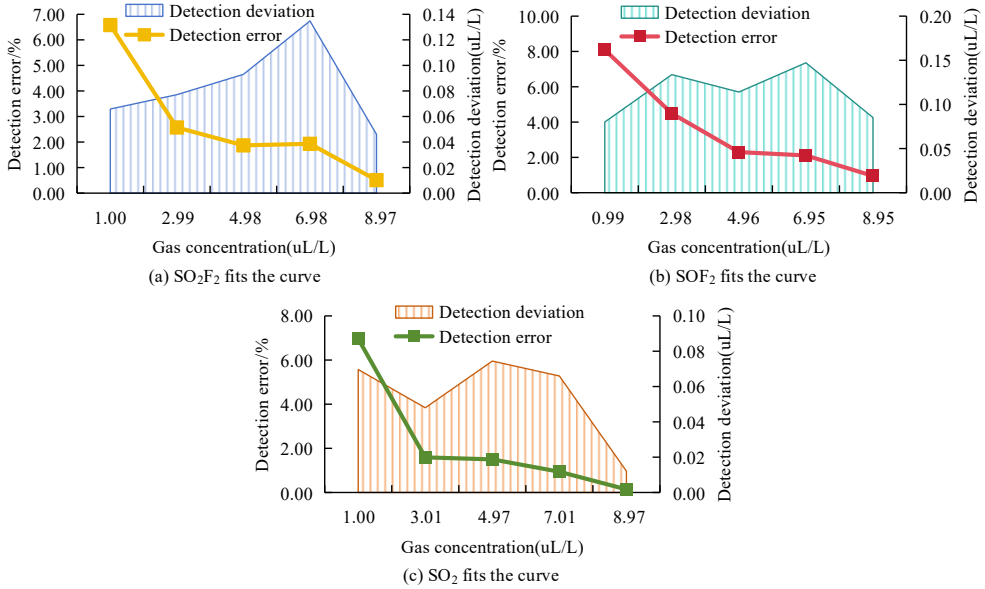

Fig. 9 Error results of gas detection at different concentrations

In Fig.s 9 (a) to (c), the maximum deviations of SO_2F_2, SOF_2, and SO_2 concentrations from the fitted concentrations are 0.0930 uL/L, 0.147uL/L, and 0.075 uL/L, with maximum errors of 6.47%, 8.11%, and 6.93%, respectively. Therefore, the platform can effectively detect trace amounts of SO_2F_2, SOF_2, and SO_2. Stability testing is vital to measure the stability of the results of a testing system over a certain period of time. The experiment conducts stability tests using 1 uL/L of SO_2F_2, SOF_2, and SO_2. The experimental environment is kept at a constant temperature, with a gas flow rate of 500 mL/min. The experimental gas goes on to detect using the experimental platform, and SHA is continuously sampled. The test results are shown in Fig. 10.

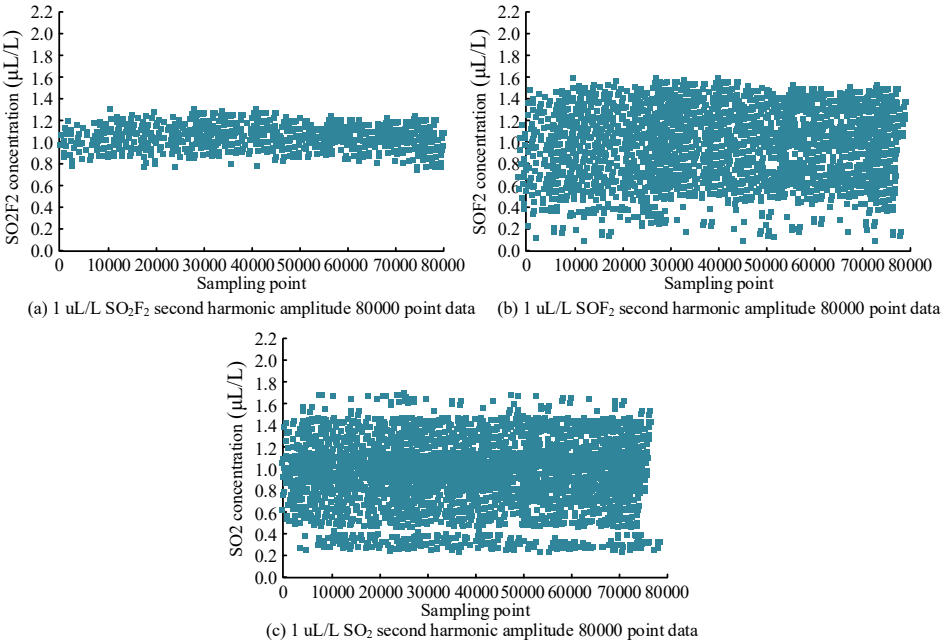

(a) 1 uL/L SO_2F_2 second harmonic amplitude 80000 point data (b) 1 uL/L SOF_2 second harmonic amplitude 80000 point data

(c) 1 uL/L SO_2 second harmonic amplitude 80000 point data

Fig. 10 SHA data of 80,000 points

In Fig. 10, among 80,000 sampled data, 85.73% of the SHA of SO_2F_2, SOF_2, and SO_2 are concentrated in the range of 1.0~1.2 uL/L, 85.10% are concentrated in the 0.8~1.3 uL/L, and 87.61% are concentrated in 0.9~1.3 uL/L. The average values of the measurement results are 0.991 uL/L, 0.969 uL/L, and 0.976 uL/L. In Fig. 10 (b), the SHA of SOF_2 and SO_2 are both between 0.3 and 1.7 uL/L. In summary, the detection systems of SO_2F_2, SOF_2, and SO_2 exhibit high stability under experimental conditions, with SHA mostly concentrated within the expected range and the average value close to the set value, verifying the stability of the experimental platform. The experiment uses 1 μL/L of SO_2F_2, SOF_2, and SO_2 as the detection gas evaluation platform to evaluate the detection effect. The gas is introduced into the detection cell at a flow of 500 mL/min and continuously

measured for 3,600s using the detection platform with a sampling rate of 50Hz. The performance of virtual phase-locked amplifiers is different from that of real phase-locked amplifiers in handling second harmonic signals. In order to verify the processing performance of the proposed virtual phase-locked amplifier, it is compared with the real phase-locked amplifier, and the specific results are shown in Table 2.

Table 2

Processing performance of different phase-locked amplifiers

Argument	Virtual phase-locked amplifier	True phase-locked amplifier
Signal to noise ratio (SNR)	2.0850	2.0050
Sensitivity (%)	98.6100	90.2360
Noise removal efficiency (%)	97.6240	89.6240
Detection limit (SO2F2)(μL/L)	0.0080	0.0100
Detection limit (SOF2)(μL/L)	0.0055	0.0060
Detection limit (SO2)(μL/L)	0.0019	0.00210

As it can be seen from Table 2, in terms of signal-to-noise ratio (SNR), the value of virtual phase-locked amplifier is 2.0850, which is slightly higher than that of real phase-locked amplifier 2.0050, indicating better signal quality. In terms of sensitivity and noise removal efficiency, the virtual phase-locked amplifier reached 98.6100% and 97.6240%, respectively, which were significantly higher than the real phase-locked amplifier's 90.2360% and 89.6240%. In addition, virtual lock-in amplifiers also show higher sensitivity in terms of detection limits, SO_2F_2, SOF_2, and SO_2 detection limits of 0.0080 μL/L, 0.0055 μL/L, and 0.0019 μL/L, respectively, which are lower than real lock-in amplifiers. Waveforms in the 2000-3500 range can be used to detect SO_2F_2. There are significant absorption inhibition features in the 2000-3200 range for the identification of SOF_2. Absorption inhibition in the range of 3250-4000 can be used as a basis for SO2 detection. The Allan Variance Curve (AVC) drawn based on the detection data is shown in Fig. 11.

In Fig. 11, the optimal integration times for SO_2F_2, SOF_2, and SO_2 are 7.76s, 44.24s, and 52.34s, corresponding to detection limits of 0.008 μL/L, 0.0055 μL/L, and 0.0019 μL/L. The results indicate that the SF_6 decomposition component detection platform built on MI TDIAS technology has an outstanding detection lower limit and is able to detect trace concentrations of SO_2F_2, SOF_2, and SO_2. In summary, by using high-resolution FTIR, the spectral characteristics of different gas molecules can be more accurately distinguished, thus reducing intermolecular interference. The characteristic absorption bands of each gas molecule are carefully selected, and these bands avoid overlapping with other gas molecules as much as possible to reduce cross interference. The improved adaptive noise whole set Empirical Mode decomposition (CEEMDAN) algorithm can effectively separate the spectral signals of different gases and improve the accuracy of detection. By

designing a virtual LiA to extract SHS, it is possible to more accurately detect the concentration of the target gas while reducing interference from other molecules.

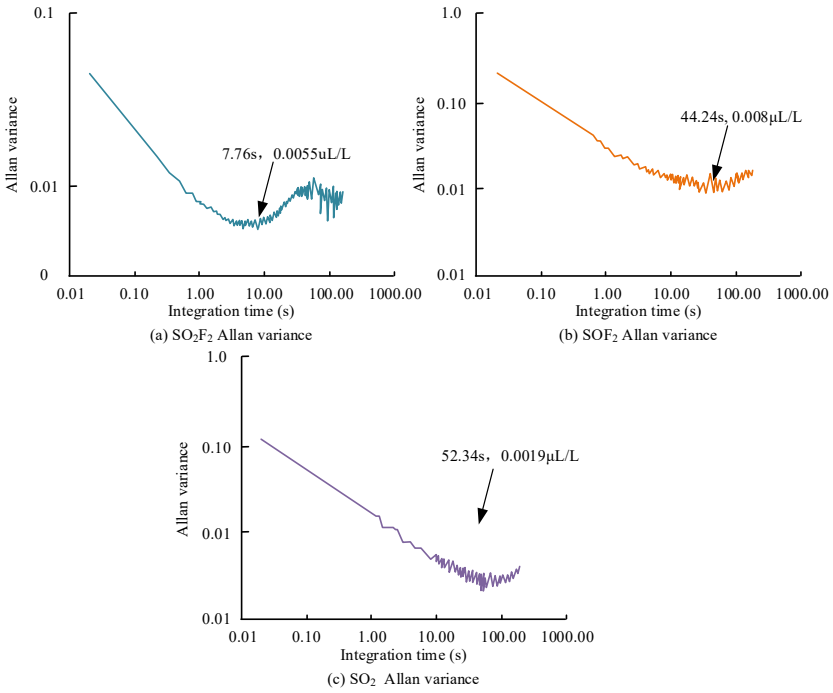

Fig. 11 AVC results

4. Discussion and Conclusion

To improve the operation reliability and prolong the service life of power equipment, the spectral data of SOF_2, SO_2F_2 and SO_2 were obtained by Fourier transform infrared spectroscopy platform, and the accuracy of the data was verified after comparison with NIST database. A virtual phase-locked amplifier (LiA) was developed based on LabVIEW, and the effects of different modulation parameters on the second harmonic signal were studied with TDLAS simulation platform. The improved CEEMDAN algorithm is used for noise degradation, and the signal-to-noise ratio of the signal is improved. The results show that the infrared detector and DAC have excellent performance, and the system can fit SO_2F_2, SOF_2 and SO_2 more than 0.98 under constant temperature condition, and the detection limits are 0.008 μL/L, 0.0055 μL/L and 0.0019 μL/L, respectively. The system showed excellent performance in trace gas detection and adaptability to complex environments. It provided reliable technical support for SF_6 gas detection in power equipment. A virtual phase-locked amplifier structure based on LabVIEW is designed for SHS. The structure can extract signals stably and reduce the influence

of environmental noise on the detection accuracy. Low frequency noise is suppressed by high frequency modulation signal, and signal extraction is optimized by modulation coefficient and frequency, so that the system can detect gas concentration effectively under the change of environment. However, the anti-interference capacity in complex environments needs to be further improved and the future research will focus on enhancing it to improve its practicality. In the future detection of sulfur hexafluoride, we will try to use VMD to first reduce the dimension and denoise of the data and then reconstruct the decomposed and filtered data through the orthogonal matching tracking (OMP) algorithm, so as to maintain the integrity of the data and improve the speed and accuracy of data processing.

REFERENCES

[1] Tian J, Zhang G, Ming C, He L, Liu Y, Liu J, Zhang X. Design of a flexible UHF Hilbert antenna for partial discharge detection in gas-insulated switchgear. IEEE Antennas and Wireless Propagation Letters, 2022, 22(4): 794-798.

[2] Chinthamu N, Karukuri M. Data Science and Applications. Journal of Data Science and Intelligent Systems, 2023, 1(1): 83-91.

[3] Rotering P, Mück-Lichtenfeld C, Dielmann F. Solvent-free photochemical decomposition of sulfur hexafluoride by phosphines: Formation of difluorophosphoranes as versatile fluorination reagents. Green Chemistry, 2022, 24(20): 8054-8061.

[4] Han X, Zhang X, Guo R, Wang H, Li J, Li Y, Zhao M. Partial discharge detection in gas-insulated switchgears using sensors integrated with UHF and optical sensing methods. IEEE Transactions on Dielectrics and Electrical Insulation, 2022, 29(5): 2026-2033.

[5] Wang Q, Fu C, Chu F, Tong Y, Wang X, Ye G, Wu X. A quantitative research on the level of disturbance to secondary signal ports of electronic voltage transformers under the operation of gas-insulated switchgear. High Voltage, 2022, 7(1): 165-175.

[6] Chu J, Wang Q, Liu Y, Pan J, Yuan H, Yang A, Xiao H W, Rong M. Fault diagnosis of SF 6-insulated equipment by micro gas sensor array. IEEE Transactions on Power Delivery, 2022, 38(1): 222-230.

[7] Wang J, Chen W, Wang P, Wan F, Zhang Z, Gao S, Wang Y. Analysis of SF6 decomposed products by fibre-enhanced Raman spectroscopy for gas-insulated switchgear diagnosis. High Voltage, 2024, 9(1): 206-216.

[8] Cheng H, Zeng F, Tang B, Li H, Tang J, Huang Z, Chao X. SF6 decomposition behaviour under partial discharge of typical insulation defects in gas-solid insulated valve-side bushing of converter transformer. High Voltage, 2023, 8(4): 690-697.

[9] Kaiyuan L I, Yuan H, Chen T, Huang L. Tunable diode laser absorption spectroscopy (TDLAS)-based optical probe initial fire detection system. Journal of Tsinghua University (Science and Technology), 2023, 63(6):910-916.

[10] Zhang Q, Zhang T, Wei Y, Liu T. Highly sensitive and reliable optical fiber TDLAS gas detection system for methane in situ monitoring in near space. Applied Optics, 2023, 62(17): 4409-4414.

[11] Chang J, He Q, Li J, Feng Q. Oxygen detection system based on TDLAS–WMS and a compact multipass gas cell. Microwave and Optical Technology Letters, 2023, 65(5):1141-1145.

[12] De S, Selvaraj R, Grattan K T V, Chakraborty A L. Detailed analysis of the R 1f/ΔI 1 WMS technique and demonstration of significantly higher detection sensitivity compared to 2f WMS for calibration-free trace gas sensing. Applied Optics, 2023, 62(12): 3160-3168.

[13] Xu Y, Wang H, Qi H, Zhao X, Guo M, Zhang Y, Chen K. High-Precision Multipass Fiber-Optic Photoacoustic Gas Analyzer Based on 2 f/1 f Wavelength Modulation Spectroscopy[J]. Analytical Chemistry, 2024, 96(6): 2543-2549.
[14] Kong W, Wan F, Lei Y, Wang C, Sun H, Wang R, Chen W. Dynamic Detection of Decomposition Gases in Eco-Friendly C5F10O Gas-Insulated Power Equipment by Fiber-Enhanced Raman Spectroscopy. Analytical chemistry, 2024, 96(38): 15313-15321.
[14] Wang Y, Gui Y, Yang J, Jin G, Yang P, Gao M, Huang H. DFT Study of Metal (Ag, Au, Pt)-Modified SnS2 for Adsorption of SF6 Decomposition Gases in Gas-Insulated Switchgear. Langmuir, 2024, 40(13): 7049-7059.
[15] Siddiqui N, Weeks C, Rogers J. Advancements in clean air insulation technologies for switchgear and circuit breakers. IEEE Power and Energy Magazine, 2022, 20(2): 132-138.
[16] Feng Z, Pan H, Yan S, Zhang B, Cheng M. Research on the 12kV Environment-friendly Intelligent Monitoring Gas-insulated Switchgear. International Core Journal of Engineering, 2023, 9(9): 120-127.
[17] Zhang B, Wang K, Yao Y, Li K, Li X, Tang N. Insulation Characteristics of HFO-1336mzz (E) and its mixtures as eco-friendly alternatives to SF 6 for medium-voltage switchgears. IEEE Transactions on Dielectrics and Electrical Insulation, 2023, 30(2): 536-545.
[18] Wang Y, Gui Y, Yang J, Jin G, Yang P, Gao M, Huang H. DFT Study of Metal (Ag, Au, Pt)-Modified SnS2 for Adsorption of SF6 Decomposition Gases in Gas-Insulated Switchgear. Langmuir, 2024, 40(13): 7049-7059.
[19] Jia C, Chu P, Zhao W, Tang Z. Characterization of internal discharge shock waves of gas-insulated switchgears using shadowgraphy. IET Generation, Transmission & Distribution, 2023, 17(24): 5378-5385.
[20] Lin M J. To research on application and maintenance of sulfur hexafluoride (SF6) circuit breaker. European Journal of Electrical Engineering and Computer Science, 2023, 7(3): 1-5.